Proc. of the 15th Int. Workshop on Slow Positron Beam Techniques and Applications, Prague, September 2–6, 2019

Early Stages of Precipitation in Mould-Cast, Cold-Rolled and Heat-Treated Aluminium Alloy AA7075 with Sc,Zr-Addition

V. Kodetová*, M. Vlach, J. Čížek, M. Cieslar, L. Bajtošová, H. Kudrnová, M. Leibner and V. Šíma

Charles University, Faculty of Mathematics and Physics, Ke Karlovu 3, 121 16 Prague, Czech Republic

Precipitation reactions of the commercial Al–Zn–Mg–Cu(–Sc–Zr) alloy in mould-cast, cold-rolled, and heat-treated states were characterized by electron microscopy, X-ray diffraction, thermal analysis, microhardness testing, and positron annihilation spectroscopy. The distinct changes in microhardness curves as well as in a heat flow of the alloys studied are mainly caused by dissolution of clusters and precipitation of particles from the Al–Zn–Mg–Cu system. An easier diffusion of Zn, Mg, and Cu atoms along dislocations is responsible for the precipitation of Zn,Mg,Cu-containing particles at lower temperatures compared to the mould-cast alloys The mould-cast and cold-rolled alloys contain solute clusters rich in Mg and Zn. Clusters formed in the heat-treated alloys during natural ageing have similar composition but in addition to Mg and Zn contain also Cu. The Cu-concentration increases with increase of period of natural ageing. The mould-cast state after natural ageing contain in addition to solute agglomerates also vacancy clusters formed by agglomeration of thermal vacancies. Addition of Sc and Zr results in a higher hardness above $\approx 270\,^{\circ}\mathrm{C}$ due to a strengthening by $Al_3(Sc,Zr)$ particles with a good thermal stability. Sc and Zr have probably no influence on the evolution of solute clusters.

DOI: 10.12693/APhysPolA.137.250

PACS/topics: 81.30.Mh, 81.40.Cd, 84.37.+q, 68.37.Lp

1. Introduction

Commercial Al–Zn–Mg–Cu-based alloys (AA7xxx series) exhibit reasonable solid solution hardening [1]. Mechanical properties of these alloys depend on a chemical composition, mainly on Zn and Mg contents and on a heat treatment of the studied alloys [2–5]. Although different authors used various notations for phases formed in the early precipitation stage, multiple publications (e.g. Refs. [2–8]) are consistent with the following precipitation sequences: (a) supersaturated solid solution (SSS) $\rightarrow$ clusters/Guinier–Preston (GP) zones $\rightarrow$ η'-phase $\rightarrow$ η-phase, (b) SSS $\rightarrow$ clusters/GP zones $\rightarrow$ T'-phase $\rightarrow$ T-phase. The η'-phase precipitates play a major role in the strengthening of the alloys [8]. But the formation of metastable precipitates depends on the alloy composition, artificial ageing temperature, ageing time, heat treatment etc. [3–5].

An addition of Sc ($\approx$ 0.2 wt%) and Zr ($\approx$ 0.1 wt%) to Al-based alloys is used to refine the cast grain structure, to increase recrystallization temperature, and to improve their mechanical properties [9, 10]. Consequently, there is an interest in a further improvement of properties of Al–Zn–Mg–Cu-based alloys containing Sc and Zr and a study of their microstructure and mechanical properties [9]. Despite the fact that the AA7xxx series alloys belong to the most extensively used Al-based alloys [4, 5, 9, 10], relatively few studies have investigated phase transformations of the Al–Zn–Mg–Cu-based alloys with Sc,Zr-addition. A tailoring of the material with required properties is very difficult without a detailed knowledge of the precipitation processes and the role of Sc and Zr in the microstructure development.

2. Experimental details

The mould-cast (MC) Al–5.4wt%Zn–3.1wt%Mg–1.5wt%Cu (7075) and Al–5.2wt%Zn–3.0wt%Mg–1.4wt%Cu–0.2wt%Sc–0.1wt%Zr (7075-ScZr) were studied. Both alloys were also cold-rolled (CR) using 21% thickness reduction. High temperature (HT) treatment of the MC alloys was performed at $475\,^{\circ}\mathrm{C}/60$ min in a furnace with an Ar protective atmosphere and was finished by a quenching.

The influence of isochronal annealing (in steps of 30 K/30 min) on mechanical properties was studied using Vickers microhardness (HV0.5) measured at $\approx 0\,^{\circ}\mathrm{C}$. To avoid a possible natural ageing (NA), after quenching, the materials were kept in liquid nitrogen at 78 K until measurements or the next annealing step. The annealing procedure was performed exactly in the same way as described in Refs. [10, 11]. The thermal behaviour of the alloys was studied using differential scanning calorimetry (DSC) performed using the heating rate of 20 K/min in the Netzsch 200 F3 Maia apparatus. Positron annihilation spectroscopy (PAS) was employed for an investigation of lattice defects. PAS measurements were performed using a ^{22}Na positron source with activity of 1 MBq sealed between 2 μm thick mylar foils. Positron

*corresponding author; e-mail: veronika.kodetova@seznam.cz

lifetime (LT) investigations were performed using a digital spectrometer [12] with a time resolution of 143 ps. Coincidence Doppler broadening (CDB) studies were carried out on a digital spectrometer [13] with an energy resolution of 0.9 keV at the annihilation line. Detailed information about measurements is described in Ref. [14]. The microstructure evolution was characterized by transmission (TEM) and scanning (SEM) electron microscopy. TEM and SEM observations were carried out in JEOL JEM 2000FX, 2200FS and MIRA I Schottky FE-SEMH microscopes. The analysis of precipitated phases was complemented by energy-dispersive spectroscopy (EDS) performed by X-ray BRUKER microanalyser.

3. Results and discussion

SEM and EDS proved presence of a Zn,Mg,Cu-containing eutectic phase at grain boundaries in the initial MC and CR state of both 7075 and 7075-Sc,Zr alloy. The initial HV0.5 values of 7075 and 7075-ScZr alloy (Fig. 1) are enhanced for CR samples due to work hardening by dislocations. Only small density of dislocations in grain interiors was observed by TEM in the MC alloys. After cold rolling the amount of dislocations rapidly increase — see Fig. 2. Although any particles (except for the eutectic phase mentioned above) were not directly

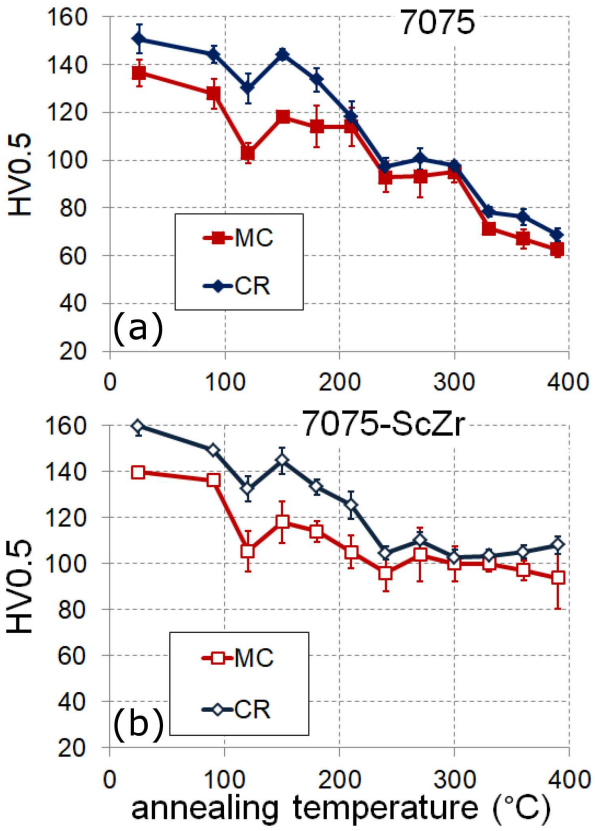

Fig. 1. Isochronal annealing HV curves of the (a) 7075 and (b) 7075-ScZr alloys.

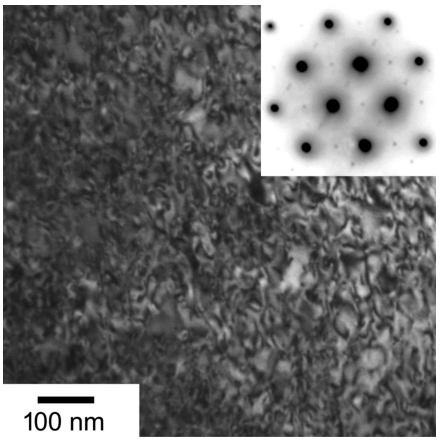

Fig. 2. TEM of the CR sample with $L1_2$ structured particles (ED pattern).

observed by TEM, the existence of the $L1_2$-structured particles was confirmed in the 7075-ScZr alloy by electron diffraction (ED), as well as some diffuse diffraction spots most probably from early precipitation stages (Fig. 2). They can be attributed to the presence of the secondary $Al_3(Sc,Zr)$ particles with $L1_2$-structure and clusters/GP zones. Thus, higher initial HV0.5 values of 7075-Sc,Zr alloy compared to 7075 one are likely due to hardening effect of the Sc,Zr-addition.

Figure 3 shows DSC curves up to 390 °C. Three processes were detected: an endothermic effect (labelled A) followed by an exothermic (B) and a slight exothermic effect (C). The maximum of the effect B is shifted to lower temperatures in the CR alloys.

Based on our previous study [8], it can be assumed that clusters/GP zones are being formed during cooling after casting and subsequent NA of the 7075(-ScZr) alloys. PAS measurements showed that positrons annihilated at traps in the MC state of the alloys are associated with small clusters characterized by a positron lifetime of 0.218–0.226 ns. This value is in a good agreement with the results reported in Ref. [15] and corresponds to positron annihilations in clusters/GP zones. Considering the isochronal HV annealing curves with a local maximum at ≈ 150 °C (see Fig. 1) and the existence of the endothermic effect A (see Fig. 3) it can be concluded that clusters/GP zones present in the MC state were dissolved during annealing 475 °C/60 min.

Figure 4a shows TEM image of the 7075-ScZr alloy in the MC state isochronally annealed up to 210 °C. Microstructure observations combined with ED and EDS proved presence of the metastable η'-phase precipitates and in addition presence of the T-phase ($Al_2Zn_3Mg_3$) and S-phase (Al_2CuMg) particles. In Al–Zn–Mg(–Cu)-based alloys the metastable η'-phase is a typical hardening phase [2–5, 8]. On the other hand, precipitation of both T- and S- phases does not lead to any significant hardening [2–6, 8]. According to the previous investigations (e.g. Refs. [8, 16, 17]) particles of the metastable η'-phase were observed at comparable tem-

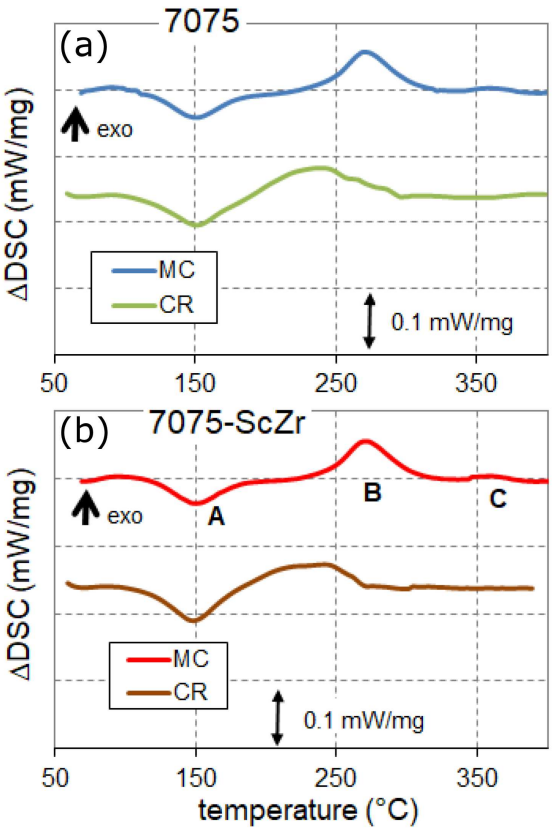

Fig. 3. DSC curves of the MC and CR alloys at heating rate of 20 K/min.

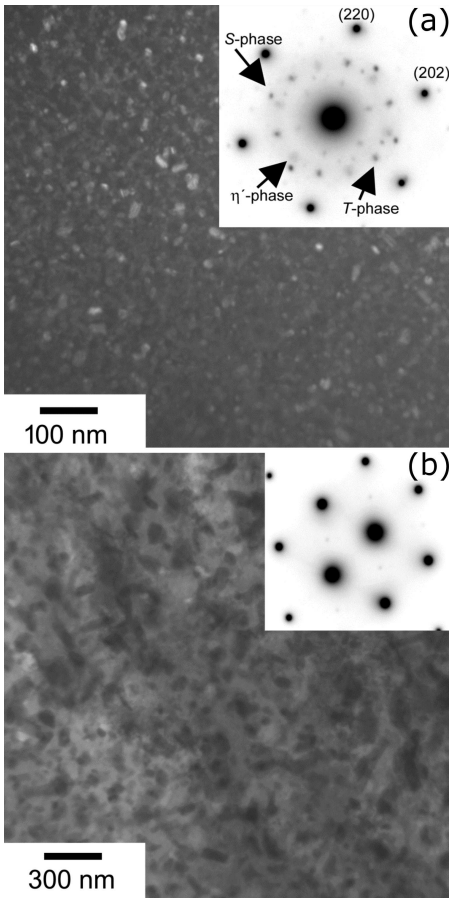

Fig. 4. TEM and ED of the (a) MC alloy annealed up to 210 °C, (b) CR alloy annealed up to 360 °C.

peratures both in AlZnMgScZr and AlZnMgCuScZr alloys. The hardening peak in the temperature range of 150–240 °C, as well as the exothermic B effect is associated with a formation of the η'-phase. It should be mentioned that possible temperature ranges of the phase transformations are often shifted to higher temperatures with increase of heating rate. This is why the exothermic peak B is located at higher temperature than the peak hardness. Maxima of the DSC peaks are shifted to lower temperatures by cold rolling which is probably caused by an easier diffusion of Mg, Zn, and Cu atoms along dislocations.

Figure 4b shows TEM image of the 7075-ScZr alloy in the CR state isochronally annealed up to 360 °C, where dispersion of the particles can be seen. These particles were identified using ED and EDS as either η- and/or T-phase. It can be concluded that the weak exothermic process C is probably related to the formation of these particles. Additional precipitation of the secondary $Al_3(Sc,Zr)$ particles was observed in the 7075-ScZr alloy — this phase was detected by ED in the 7075-ScZr samples annealed up to 360 °C (see Fig. 4b). The precipitation of $Al_3(Sc,Zr)$ particles is the reason for a more pronounced hardening of the alloy with Sc,Zr-addition, see Fig. 1.

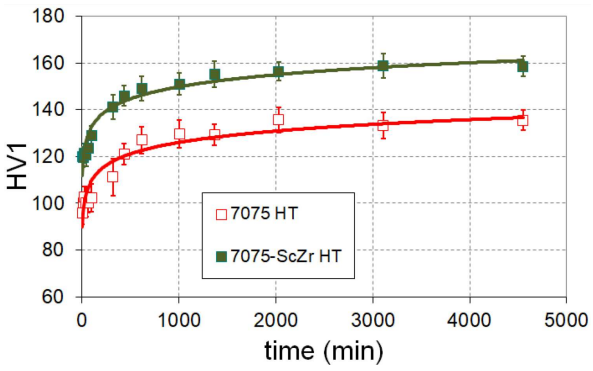

Fig. 5. HV evolution of the HT alloys during NA.

Figure 5 shows the variations of the microhardness during NA of the HT alloys. HV increases immediately after quenching to room temperature. Higher HV values of 7075-ScZr alloy reflect strengthening due to Sc,Zr-addition. From comparison of the HV0.5 values of MC and HT alloys (cf. Figs. 1 and 5) it can be concluded that clusters/GP zones are dissolved during the heat treatment at 475 °C/60 min. Owing to the strengthening effect of clusters/GP zones, HV0.5

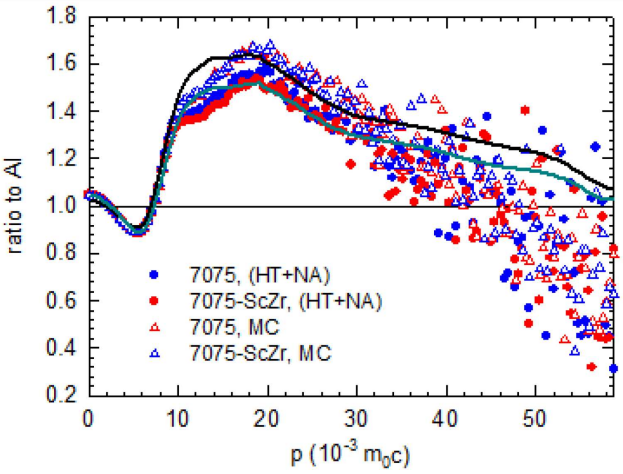

Fig. 6. CDB ratio curves (related to well annealed Al) for 7075 and 7075-ScZr alloys in the MC state and HT state after NA (HT+NA). Solid lines represent superposition of contributions of positrons annihilated by pure elements Al, Zn, Mg and Cu.

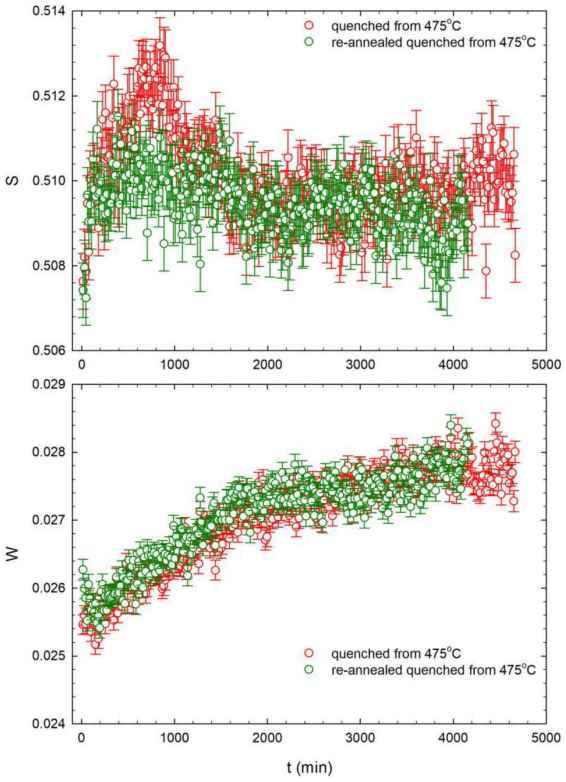

Fig. 7. The development of S and W parameter of 7075-ScZr alloy during NA.

increases continuously during NA due to the formation of solute clusters. This is in agreement with other studies of Al–Zn–Mg(–Cu)-based alloys (e.g. Ref. [8]).

LT spectra of the HT alloys after NA consist of two components: (i) a shorter component with a lifetime $\tau_1 \approx 221$ ps and intensity $I_1 \approx 91\%$ represents a contribution of positrons trapped at Zn,Mg(Cu)-containing solute clusters; (ii) a longer component with lifetime $\tau_2 \approx 440$ ps and intensity $I_2 \approx 9\%$ comes from positrons trapped at vacancy clusters. Figure 6 shows the CDB ratio curves (related to pure Al) of 7075 and 7075-ScZr alloys in the MC state and in the HT state after NA. One can see in the figure that the ratio curves for 7075 and 7075-ScZr alloys are almost the same. It indicates that addition of Sc and Zr has negligible influence on positron trapping. Solutes of Sc and Zr are, thereby, not incorporated into solute clusters formed during NA or cooling after casting. Note that $Al_3(Sc,Zr)$ particles do not represent positron trapping sites [14]. There is, however, a difference between ratio curves for alloys in the MC state and in the HT state after NA. The CDB ratio curves of 7075 and 7075-ScZr alloys can be well described assuming that positrons are annihilated in the vicinity of Zn (28%) and Mg (25%) atoms for the MC alloys and Zn (27%), Mg (18%), and Cu (4%) atoms for the HT alloys after NA. The fractions of positrons annihilated in the vicinity of Mg, Zn, and Cu atoms are clearly substantially higher than the concentrations of these elements in the alloy. This indicates that the local chemical environment of positron traps is enriched in Mg, Zn, and Cu, i.e., coherent clusters were formed predominantly by these elements.

Figure 7 shows the development of the S and W parameter during NA of the 7075-ScZr alloy in the HT state and re-annealed state. From inspection of Fig. 7 one can conclude that at the beginning of NA parameter S increases first and it is accompanied by a decrease of W. After reaching a local maximum at NA period of ≈ 720 min parameter S decreases again and it is accompanied by gradual increase of W. Hence, in early stages of NA solute clusters with imperfect structure containing vacancies are formed. This is reflected by an increase of S and a decrease of W. Later the development of solute clusters takes place, their structure is improved and vacancies are gradually removed. This leads to subsequent drop of S after reaching a local maximum at ≈ 720 min. With increasing NA period the composition of solute clusters develops. Most probably the clusters become enriched in Cu which is reflected by a gradual increase of W. After NA the samples were re-annealed at 475 °C/60 min and NA was repeated. One can see that the development of S and W parameters after re-annealing is similar to that in the first NA cycle.

The LT spectra of samples after NA consist of two components: (i) a contribution of positrons trapped at solute clusters with lifetime of $\tau_1 \approx 222$ ps and intensity $I_1 \approx 96\%$, and (ii) a component with lifetime $\tau_2 \approx 480$ ps and intensity $I_2 \approx 5\%$ representing a contribution of positrons trapped at vacancy clusters. Hence, comparing with samples in the MC state LT spectra exhibit similar components but intensity of the component corresponding to vacancy clusters is slightly lower. This indicates that solute clusters formed during NA are similar to those in the mould-cast samples.

4. Conclusions

Results of characterization of mould-cast, cold-rolled, and heat-treated alloys can be summarized in the following points:

- The initial microhardness values of the alloys reflect the cold rolling. Easier diffusion of Zn, Mg, and Cu atoms along dislocations in the cold-rolled alloys is responsible for the precipitation of Zn,Mg,Cu-containing particles at the lower temperatures compared to the mould-cast alloys.
- The distinct changes in microhardness curves, as well as in the heat flow of the alloys are mainly caused by the dissolution of clusters/GP zones and precipitation of particles from the Al–Zn–Mg–Cu system. Strengthening effect due to the formation of GP zones and/or growing of clusters is observed during natural ageing.
- Addition of Sc,Zr results in a higher hardness above $\approx 270\,^{\circ}\mathrm{C}$ due to the strengthening by Al_3(Sc,Zr) particles.
- CDB investigations revealed that mould-cast alloys contain solute clusters rich in Mg and Zn. Solute clusters formed in the heat-treated alloys during natural ageing have similar composition but in addition to Mg and Zn contain also Cu. The concentration of Cu in solute clusters increases with increase of period of natural ageing. Addition of Sc and Zr has no influence on the development of solute clusters. LT investigations revealed that alloys in the mould-cast state and after natural ageing contain in addition to solute agglomerates also vacancy clusters formed by agglomeration of thermal vacancies.

Acknowledgments

This work was supported by The Czech Science Foundation (GACR, project no. 17-17139S). Authors are also grateful to Bohumil Smola for his experimental help.

References

[1] T. Dursun, C. Soutis, *Mater. Des.* **56**, 862 (2014).
[2] K.R. Prasanta, M.M. Ghosh, K.S. Ghosh, *Mater. Character.* **104**, 49 (2015).
[3] N. Afify, A. Gaber, G. Abbady, *Mater. Sci. Appl.* **2**, 427 (2011).
[4] K.S. Ghosh, N. Gao, M.J. Starink, *Mater. Sci. Eng. A* **552**, 164 (2012).
[5] K.S. Ghosh, N. Gao, *Trans. Non-Met. Soc. China* **21**, 1199 (2011).
[6] C. Antonione, F. Marino, G. Riontino, S. Abis, E. Russo, *Mater. Chem. Phys.* **20**, 13 (1988).
[7] S. Abis, G. Riontino, *Mater. Lett.* **5**, 442 (1987).
[8] M. Vlach, V. Kodetová, B. Smola, J. Čížek, T. Kekule, M. Cieslar, H. Kudrnová, L. Bajtošová, M. Leibner, I. Procházka, *Kovové Mater.-Metall. Mater.* **56**, 367 (2018).
[9] L.S. Toropova, D.G. Eskin, M.L. Kharakterova, T.V. Dobatkina, in: *Advanced Aluminium Alloys Containing Scandium–Structure and Properties*, Gordon and Breach Science Publisher, The Netherlands, 1998.
[10] M. Vlach, I. Stulíková, B. Smola, T. Kekule, H. Kudrnová, V. Kodetová, V. Očenášek, J. Málek, V. Neubert, *Kovové Mater.-Metallic Mater.* **53**, 295 (2015).
[11] J. Čížek, I. Procházka, B. Smola, I. Stulíková, M. Vlach, V. Očenášek, O.B. Kulyasova, R.K. Islamgaliev, *Int. J. Mater. Res.* **100**, 6 (2009).
[12] F. Bečvář, J. Čížek, I. Procházka, J. Janotová, *Nucl. Inst. Methods Phys. Res. A* **539**, 372 (2005).
[13] J. Čížek, M. Vlček, I. Procházka, *Nucl. Instrum. Methods Phys. Res. A* **623**, 982 (2010).
[14] M. Vlach, J. Čížek, O. Melikhova, I. Stulíková, B. Smola, T. Kekule, H. Kudrnová, R. Gemma, V. Neubert, *Metall. Mater. Trans. A* **46**, 1556 (2015).
[15] G. Dlubek, R. Krause, O. Brommer, *J. Mater. Sci.* **21**, 853 (1986).
[16] P. Lang, T. Wojcik, E. Povoden-Karadeniz, A. Falahati, E. Kozeschnik, *J. Alloys Comp.* **609**, 129 (2014).
[17] J. Tang, H. Chen, X. Zhang, S. Liu, W. Liu, H. Ouyang, H. Li, *Trans. Nonferr. Met. Soc. China* **22**, 1255 (2012).